Enhancing the Dynamic Performance of a Standalone DFIG Under Variable Speed Operation Using an Effective Control Technique

Mahmoud K. Abdelhamid[1], Mahmoud A. Mossa[2], Ahmed A. Hassan[3]

Assistant Lecture Electrical Engineering Department, Faculty of Engineering, Minia University, Minia 61111, Egypt[1]
Assistant Professor Electrical Engineering Department, Faculty of Engineering, Minia University, Minia 61111, Egypt[2]
Professor Electrical Engineering Department, Faculty of Engineering, Minia University, Minia 61111, Egypt[3]

A R T I C L E I N F O	A B S T R A C T
	The paper aims at introducing an efficient control algorithm which enhances the dynamic performance of a standalone doubly fed induction generator (DFIG) operating at variable speeds. To illustrate the effectiveness of the proposed controller, the performance of the DFIG is also evaluated using other control strategies. The control approaches which are used for the comparison purpose are the stator voltage-oriented control (SVOC) and the model predictive direct torque control (MPDTC). At first, the performance of the DFIG under each control technique is analyzed in details, showing the principle of operation of each strategy; then, a comprehensive dynamic performance comparison is performed among the three controllers; through which the merits and defects of each technique are clarified. The results confirm the validation and superiority of the proposed predictive voltage control (PVC) strategy over the other control techniques. This is illustrated through the faster dynamics, the simplicity, the reduced computational efforts and reduced ripples content. Moreover, the numerical results are showing a reduction in the total harmonic distortion (THD) with a percentage of 1.72% compared to MPDTC, and also showing a faster dynamic response in the power and torque profiles with percentage of 0.98% and 0.7% compared to SVOC; and with percentage of 0.1% and 0.52% compared to MPDTC, respectively.

1. Introduction

As the availability of the non-renewable energy resources is decreasing day by day, there is a severe need for finding new control approaches which can extract maximum power from renewable energy resources, such as wind, solar, hydropower, biomass and geothermal energies [1]. Doubly fed Induction Generators (DFIGs) have been widely utilized with renewable energy sources especially wind energy, which known as wind energy conversion system (WECS) [2]. There are two categories of wind turbines which used in WECS: fixed speed wind turbines and variable speed wind turbines [3]. In fixed speed wind turbines, synchronous generator can be used where the speed control can be performed with the aid of gear ratio of the gear box in between the turbine and the generator's shaft; but this type has a substantial defect: the mechanical losses are very high which leads to reducing the efficiency of the energy conversion process [4, 5]. On the other hand, variable speed wind turbines use DFIG with back to back converter in between stator and rotor windings which eliminates the need to gear ratio control [6].

The ability of the DFIG to generate constant output voltages with constant frequency during variable wind speeds, is considered as the main motive to be used with wind turbines [7]. In addition, the DFIG can be either controlled from the rotor side or the stator side, which makes its control simple and flexible [8, 9]. Usually, the DFIG is controlled from the rotor side to be able to minimize the power rating of the power electronic switches used in the converters, as the rating is selected based on the slip power instead of the stator power, this leads to minimizing the cost and losses of the used converters [10].

The designers' efforts are still directed towards developing control methods and finding the best method capable of achieving optimal dynamic performance for the DFIG [11, 12]. The vector orientation control (VOC) is adopted in [13, 14], which has managed to minimize the ripples' content and enhance the response of the torque, on the other hand the VOC still suffers from its dependence on the model parameters and requiring coordinate transformations [15]. Furthermore, the system is complex and suffers from a delay in its dynamic response as it uses PI regulators [16]. In [17, 18], the direct torque control (DTC) approach is utilized, which utilizes hysteresis torque and rotor flux comparator instead of PI regulators, thus, it has succeeded in overcoming the VOC's complexity and getting a fast-dynamic response [19]. Finally, the predictive control (PC) strategy came to overcoming the defects which face the VOC and DTC [20]. It utilizes a cost function instead of the current control loops and PI regulators which are used in VOC and the hysteresis comparators which are adopted by DTC [21]. The PC managed to getting a fast-dynamic response, reducing the complexity and minimizing the ripples' content [22].

The contributions of the presented study can be summarized as follows:

- The article introduces a detailed design for an efficient PVC scheme which succeeded in avoiding the defects of the previous control techniques.
- The article provides a comprehensive dynamic performance analysis for the DFIG with the proposed PVC approach and the other control strategies under different operating speeds; also, the operating principle of each strategy is clarified in details.

The present article is arranged as following: At first, the mathematical model of the DFIG is introduced, then, the base principle of the adopted controllers and the performance of the DFIG with each controller are described. Subsequently, the test results are presented for each strategy with related analysis, and finally, the conclusions are summarized.

2. Mathematical Model of DFIG

As shown in Figure 1, the model of the DFIG is constructed. As the SVOC is adopted here, so, all variables are expressed in a frame which revolves with a speed analogous to the stator voltage vector's speed $(\omega_{\bar{u}_{s,k}})$.
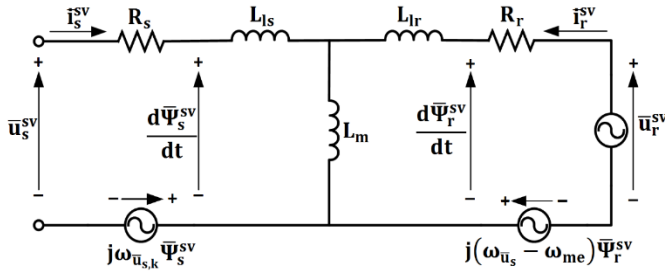
Figure 1: Equivalent circuit of DFIG

The state variables of Figure 1, are represented in discrete form at instant KT_s; where T_s is the sampling time; the dynamics of the DFIG can be represented by the following equations:

$$\frac{d\bar{\Psi}_{ds,k}^{sv}}{dt} = \bar{u}_{ds,k}^{sv} - R_s \bar{\imath}_{ds,k}^{sv} + \omega_{\bar{u}_{s,k}} \bar{\Psi}_{qs,k}^{sv} \tag{1}$$

$$\frac{d\bar{\Psi}_{qs,k}^{sv}}{dt} = \bar{u}_{qs,k}^{sv} - R_s \bar{\imath}_{qs,k}^{sv} - \omega_{\bar{u}_{s,k}} \bar{\Psi}_{ds,k}^{sv} \tag{2}$$

$$\frac{di_{dr,k}^{sv}}{dt} = \frac{L_m^2 + L_r L_t}{L_r^2 L_t}\left[u_{dr,k}^{sv} - R_r i_{dr,k}^{sv}\right.$$
$$\left. + \frac{L_r}{L_m}\omega_{slip,k}\left(\Psi_{qs,k}^{sv} - L_t i_{qs,k}^{sv}\right)\right]$$
$$- \frac{L_m}{L_r L_t}\left(u_{ds,k}^{sv} - R_s i_{ds,k}^{sv}\right.$$
$$\left. + +\omega_{\bar{u}_{s,k}}\Psi_{qs,k}^{sv}\right) \tag{3}$$

$$\frac{di_{qr,k}^{sv}}{dt} = \frac{L_m^2 + L_r L_t}{L_r^2 L_t}\left[u_{qr,k}^{sv} - R_r i_{qr,k}^{sv}\right.$$
$$\left. - \frac{L_r}{L_m}\omega_{slip,k}\left(\Psi_{ds,k}^{sv} - L_t i_{ds,k}^{sv}\right)\right]$$
$$- \frac{L_m}{L_r L_t}\left(u_{qs,k}^{sv} - R_s i_{qs,k}^{sv}\right.$$
$$\left. - -\omega_{\bar{u}_{s,k}}\Psi_{ds,k}^{sv}\right) \tag{4}$$

The d-q components of the stator flux linkage can be obtained using equations (1) and (2), while the rotor current d-q components can be evaluated using equations (3) and (4).

The stator and rotor flux linkages can be expressed in the d-q axes as following:

$$\Psi_{ds,k}^{sv} = L_s i_{ds,k}^{sv} + L_m i_{dr,k}^{sv} \tag{5}$$

$$\Psi_{qs,k}^{sv} = L_s i_{qs,k}^{sv} + L_m i_{qr,k}^{sv} \tag{6}$$

$$\Psi_{dr,k}^{sv} = L_r i_{dr,k}^{sv} + L_m i_{ds,k}^{sv} \tag{7}$$

$$\Psi_{qr,k}^{sv} = L_r i_{qr,k}^{sv} + L_m i_{qs,k}^{sv} \tag{8}$$

The mechanical equation of the DFIG can be formulated as:

$$\frac{d\omega_{me,k}}{dt} = \frac{p}{J}\left(T_{me,k} - T_{d,k}\right) \tag{9}$$

The torque developed by the DFIG can be represented as follows:

$$T_{d,k} = 1.5 p L_m \left(i_{dr,k}^{sv} i_{qs,k}^{sv} - i_{qr,k}^{sv} i_{ds,k}^{sv}\right) \tag{10}$$

The superscript $'sv'$ denotes that all variables are represented in the stator voltage frame which revolves with the synchronous angular speed $(\omega_{\bar{u}_s})$; ω_{me} and ω_{slip} refer to the rotor angular speed and slip speed, respectively. The parameters R_s, R_r are referring to the stator and rotor resistances; meanwhile L_s, L_r, L_m and L_t are the stator, rotor, mutual and transient inductances respectively. p, J, and T_{me} denote the number of pole pairs, moment of inertia and applied mechanical torque respectively.

3. Control Techniques of DFIG

3.1. SVOC Technique

The SVOC approach is introduced clearly in [10, 23]. The reference frames are shown in Figure 2, in which the stator voltage vector $\bar{u}_{s,k}$ is oriented with the *d*-axis of the synchronous frame.

Figure 2: Reference frames

Figure 3: Scheme of SVOC strategy

Thus, under SVOC, we can conclude that:

$$u_{ds,k}^{sv} = \left|\bar{u}_{s,k}^{sv}\right| \qquad \text{and} \qquad u_{qs,k}^{sv} = 0 \qquad (11)$$

$$\Psi_{ds,k}^{sv} \approx 0.0 \qquad \text{and} \qquad \Psi_{qs,k}^{sv} \approx -\frac{u_{ds,k}^{sv}}{\omega_{\bar{u}_{s,k}}} \qquad (12)$$

So, the stator current components can be expressed in terms of rotor current components as follows:

$$i_{ds,k}^{sv} = -\left(\frac{L_m}{L_s}\right) i_{dr,k}^{sv} \qquad (13)$$

$$i_{qs,k}^{sv} = \frac{\Psi_{qs,k}^{sv}}{L_s} - \left(\frac{L_m}{L_s}\right) i_{qr,k}^{sv} = -\left(\frac{L_m}{L_s}\right) i_{qr,k}^{sv} - \frac{u_{ds,k}^{sv}}{\omega_{\bar{u}_{s,k}} L_s} \qquad (14)$$

As stated in [10], the rotor voltage balance equations can be represented as follows:

$$u_{dr,k}^{sv} = \overbrace{R_r i_{dr,k}^{sv} + \sigma L_r \frac{d i_{dr,k}^{sv}}{dt}}^{u'_{dr,k} = \text{Active Term}}$$
$$- \overbrace{\omega_{slip,k}\left(\frac{L_m}{L_s}\Psi_{qs,k}^{sv} + \sigma L_r i_{qr,k}^{sv}\right)}^{\Delta u_{dr,k}^{sv} = \text{Compensation Term}} \qquad (15)$$

$$u_{qr,k}^{sv} = \overbrace{R_r i_{qr,k}^{sv} + \sigma L_r \frac{d i_{qr,k}^{sv}}{dt}}^{u'_{qr,k} = \text{Active Term}}$$
$$+ \overbrace{\omega_{slip,k}\sigma L_r i_{dr,k}^{sv}}^{\Delta u_{qr,k}^{sv} = \text{compensation term}} \qquad (16)$$

The schematic diagram of the SVOC is shown in Figure 3, in which the reference rotor current components are obtained using the errors of the load active power and load voltage with the aid of two PI regulators to provide the required load power and maintain a constant load voltage all time which is considered as an important requirement for standalone systems. Also, it's necessary to keep the frequency of the load voltage constant, so, the reference frequency is utilized to calculate the synchronous angular speed $(\omega_{\bar{u}_s})$ and the stator voltage angle $(\theta_{\bar{u}_s})$.

3.2. MPDTC Technique

The MPDTC strategy is presented in a detailed manner in [10, 19]. The adopted cost function can be formulated as:

$$C^i = \left|T_{e,k+1}^* - T_{e,k+1}\right|^i + \omega_f \left|\left|\bar{\Psi}_{r,k+1}^*\right| - \left|\bar{\Psi}_{r,k+1}^{sv}\right|\right|^i \qquad (17)$$

Where the sectors (0, …., 7) are denoted by the superscript [i].

As noted, equation (17) contains variables which depends in its evaluation on the machine parameters which can be affected by the operating conditions, also, it requires a weighting factor (ω_f). Furthermore, the torque and rotor flux values are evaluated and predicted to be utilized in the cost function, which leads to increase the computational burden.

The scheme of the MPDTC is introduced in Figure 4. As mentioned previously, the stator voltage angle $(\theta_{\bar{u}_s})$ is obtained using the reference frequency, then $(\theta_{\bar{u}_{s,k+1}})$ can be calculated using the following formulation:

$$\theta_{\bar{u}_{s,k+1}} = \theta_{\bar{u}_{s,k}} + \left(\frac{\theta_{\bar{u}_{s,k}} - \theta_{\bar{u}_{s,k-1}}}{\Delta T}\right) T_s \qquad (18)$$

The rotor position $(\theta_{me,k+1})$ can be evaluated as follows:

$$\theta_{me,k+1} = \theta_{me,k} + \left(\frac{\theta_{me,k} - \theta_{me,k-1}}{\Delta T}\right) T_s \qquad (19)$$

The actual predicted components of the rotor current can be found utilizing Taylor expansion as following:

$$i_{dr,k+1}^{sv} = i_{dr,k}^{sv} + \left(\frac{d i_{dr,k}^{sv}}{dt}\right) T_s \qquad (20)$$

$$i_{qr,k+1}^{sv} = i_{qr,k}^{sv} + \left(\frac{d i_{qr,k}^{sv}}{dt}\right) T_s \qquad (21)$$

The derivative components of the rotor current can be calculated using equations (3) and (4). The stator current predicted components $i_{ds,k+1}^{sv}$ and $i_{qs,k+1}^{sv}$ can be evaluated in the same manner. The actual predicted value of the torque can be

calculated utilizing equation (10), while the rotor flux can be evaluated as following:

$$\left|\overline{\Psi}_{r,k+1}^{sv}\right| = \sqrt{\left(\Psi_{dr,k+1}^{sv}\right)^2 + \left(\Psi_{qr,k+1}^{sv}\right)^2} \qquad (22)$$

The reference components of the stator current can be evaluated using equations (13) and (14), then the reference torque $T_{e,k+1}^*$ can be calculated as follows:

$$T_{e,k+1}^* = 1.5pL_m\left(i_{dr,k}^* i_{qs,k}^* - i_{qr,k}^* i_{ds,k}^*\right) \qquad (23)$$

The reference rotor flux $\left|\overline{\Psi}_{r,k+1}^*\right|$ can be found as following:

$$\left|\overline{\Psi}_{r,k+1}^*\right| = \sqrt{\left(\Psi_{dr,k+1}^*\right)^2 + \left(\Psi_{qr,k+1}^*\right)^2} \qquad (24)$$

Figure 4: Scheme of MPDTC strategy

3.3. Proposed PVC Technique

The cost function adopted in the proposed PVC approach is expressed by:

$$\Lambda^i = \left|u_{dr,k+1}^* - u_{dr,k+1}^{sv}\right|^i + \left|u_{qr,k+1}^* - u_{qr,k+1}^{sv}\right|^i \qquad (25)$$

As it's clear from equation (25), the utilized cost function is very simple, as its components doesn't depend on the model parameters, moreover, it doesn't need a weighting scale because it consists of two analogous terms, which are the differences between the reference and predicted values of the rotor voltage. The predicted components of the rotor voltage $\left(u_{dr,k+1}^{sv}\right)$ and $\left(u_{qr,k+1}^{sv}\right)$ are obtained utilizing the switching states of the voltage source inverter (VSI), while the reference rotor voltage components $\left(u_{dr,k+1}^*\right)$ and $\left(u_{qr,k+1}^*\right)$ can be calculated using the errors of the torque and air-gap energy with the aid of two PI regulators, which are designed as following:

As mentioned in [19], the torque derivative $\left(T_{e,k+1}\right)$ can be represented by:

$$\frac{dT_{e,k+1}}{dt} = -1.5p\frac{L_m}{\sigma L_s L_r}\left(\frac{L_m}{L_r}\Psi_{qr,k+1}^{sv}u_{dr,k}^{sv} + \Psi_{dr,k+1}^{sv}u_{ds,k+1}^{sv}\right)$$
$$- \left(\frac{R_s}{\sigma L_s} + \frac{R_r}{\sigma L_r}\right)T_{e,k+1}$$
$$- \frac{L_m}{L_r}\omega_{me,k+1}\left(\Psi_{qr,k+1}^{sv}\right)^2 \qquad (26)$$

The air-gap energy (E_{k+1}) and its derivative $\left(\frac{dE_{e,k+1}}{dt}\right)$ can be formulated as:

$$E_{k+1} = 1.5p\frac{L_m}{\sigma L_s L_r}\left(\Psi_{ds,k+1}^{sv}\Psi_{dr,k+1}^{sv} + \Psi_{qs,k+1}^{sv}\Psi_{qr,k+1}^{sv}\right) \qquad (27)$$

$$\frac{dE_{e,k+1}}{dt} = 1.5p\frac{L_m}{\sigma L_s L_r}\left[\Psi_{qs,k+1}^{sv}u_{qr,k+1}^{sv}\right.$$
$$- \left(\frac{R_s}{\sigma L_s} + \frac{R_r}{\sigma L_r}\right)\Psi_{qs,k+1}^{sv}\Psi_{qr,k+1}^{sv}$$
$$+ \frac{R_s L_m}{\sigma L_s L_r}\left(\left(\Psi_{qs,k+1}^{sv}\right)^2 + \left(\Psi_{qr,k+1}^{sv}\right)^2\right)$$
$$\left. - \omega_{slip,k+1}\Psi_{qs,k+1}^{sv}\Psi_{dr,k+1}^{sv}\right] \qquad (28)$$

The d-axis component of the rotor flux can be represented by:

$$\Psi_{dr,k}^{sv} = \frac{L_m}{L_s}\Psi_{ds,k}^{sv} + \sigma L_r i_{dr,k}^{sv} \qquad (29)$$

As known, $\Psi_{ds,k}^{sv} \approx 0.0$ under SVOC, also, the rotor transient inductance (σL_r) is very small and can be neglected, so we can consider that:

$$\Psi_{dr,k}^{sv} = 0 \qquad \text{and} \qquad \Psi_{qr,k}^{sv} = \left|\overline{\Psi}_{r,k}^{sv}\right| \qquad (30)$$

Assuming that, $K = 1.5p\frac{L_m}{\sigma L_s L_r}$, $K' = K\frac{L_m}{L_r}\Psi_{qr,k+1}^{sv}$, $K_1 = \frac{R_s}{\sigma L_s} + \frac{R_r}{\sigma L_r}$, $K_2 = \frac{L_m}{L_r}\omega_{me,k+1}\left(\Psi_{qr,k+1}^{sv}\right)^2$ and $K_3 = \frac{R_s L_m}{\sigma L_s L_r}$

Equation (24) can be reformulated as:

$$\frac{dT_{e,k+1}}{dt} = -\left(K\frac{L_m}{L_r}\Psi_{qr,k+1}^{sv}\right)u_{dr,k}^{sv} - K_1 T_{e,k+1} - K_2$$

$$\frac{dT_{e,k+1}}{dt} = -K'u_{dr,k}^{sv} - K_1 T_{e,k+1} - K_2$$

$$K'u_{dr,k}^{sv} = -K_1 T_{e,k+1} - \frac{dT_{e,k+1}}{dt} - K_2$$

$$u_{dr,k}^{sv} = \underbrace{-\frac{K_1}{K'}T_{e,k+1} - \frac{1}{K'}\frac{dT_{e,k+1}}{dt}}_{u_{dr,k+1}' = Active\ term}$$
$$\underbrace{- \frac{K_2}{K'}}_{\Delta u_{dr,k+1}^{sv} = Compensation\ term} \qquad (31)$$

$$u_{dr,k+1}' = -\frac{K_1}{K'}T_{e,k+1} - \frac{1}{K'}\frac{dT_{e,k+1}}{dt} \qquad (32)$$

Equation (28) can be reformulated as:

$$\frac{dE_{e,k+1}}{dt} = k\Psi_{qs,k+1}^{sv}u_{qr,k+1}^{sv} - K_1\Psi_{qs,k+1}^{sv}\Psi_{qr,k+1}^{sv}$$
$$+ K_3\left(\left(\Psi_{qs,k+1}^{sv}\right)^2 + \left(\Psi_{qr,k+1}^{sv}\right)^2\right)$$

$$1.2ku_{qr,k+1}^{sv} = -\frac{dE_{e,k+1}}{dt} + 1.44K_1 - 2.88K_3$$

$$u_{qr,k+1}^{sv} = \underbrace{-\frac{1}{1.2k}\frac{dE_{e,k+1}}{dt}}_{u'_{qr,k+1} = Active\ term}$$

$$+ \underbrace{1.2\frac{K_1}{k} - 2.4\frac{K_3}{k}}_{\Delta u_{qr,k+1}^{sv} = Compensation\ term} \quad (33)$$

$$u'_{qr,k+1} = -\frac{1}{1.2k}\frac{dE_{e,k+1}}{dt} \quad (34)$$

By applying Laplace transform to equations (32) and (34), assuming the initial torque and air gap energy to be zero.

$$u'_{dr,k+1}(s) = -\frac{K_1}{K'}T_{e,k+1}(s) - \frac{1}{K'}\left[sT_{e,k+1}(s) - T_{e,k+1}(0)\right]$$

$$u'_{dr,k+1}(s) = T_{e,k+1}(s)\left(\frac{-K_1 - s}{K'}\right)$$

$$\frac{T_{e,k+1}(s)}{u'_{dr,k+1}(s)} = \left(\frac{-K_1 - s}{K'}\right) \quad (35)$$

In the same manner, we can obtain: $\frac{E_{e,k+1}(s)}{u'_{qr,k+1}(s)} = -\frac{1.2k}{s}$ (36)

The transfer functions of the of the PI regulators can be expressed as:

$$u'_{dr,k+1}(s) = \overbrace{\left(k_p + \frac{k_i}{s}\right)}^{PI}\overbrace{\left[T_{e,k+1}^*(s) - T_{e,k+1}(s)\right]}^{d-current\ error} \quad (37)$$

$$u'_{qr,k+1}(s) = \underbrace{\left(k_p + \frac{k_i}{s}\right)}_{PI}\underbrace{\left[E_{e,k+1}^*(s) - E_{e,k+1}(s)\right]}_{q-current\ error} \quad (38)$$

By dividing both sides of equations (37) and (38) on $T_{e,k+1}(s)$ and $E_{e,k+1}(s)$, respectively, it results:

$$\frac{u'_{dr,k+1}(s)}{T_{e,k+1}(s)} = \left(\frac{k_p s + k_i}{s}\right)\left[\frac{T_{e,k+1}^*(s)}{T_{e,k+1}(s)} - 1\right] \quad (39)$$

$$\frac{u'_{qr,k+1}(s)}{E_{e,k+1}(s)} = \left(\frac{k_p s + k_i}{s}\right)\left[\frac{E_{e,k+1}^*(s)}{E_{e,k+1}(s)} - 1\right] \quad (40)$$

By substituting the term $\{u'_{dr,k+1}(s)\}$ from (35) into (39), we can obtain:

$$\frac{T_{e,k+1}(s)}{T_{e,k+1}(s)}\left(\frac{s + K_1}{-K'}\right) = \left(\frac{k_p s + k_i}{s}\right)\left[\frac{T_{e,k+1}^*(s)}{T_{e,k+1}(s)} - 1\right]$$

$$\frac{s + K_1}{-K'} = \left(\frac{k_p s + k_i}{s}\right)\left[\frac{T_{e,k+1}^*(s)}{T_{e,k+1}(s)}\right] - \frac{k_p s + k_i}{s}$$

$$\frac{k_p s + k_i}{s}\left[\frac{T_{e,k+1}^*(s)}{T_{e,k+1}(s)}\right] = \frac{k_p s + k_i}{s} - \frac{s + K_1}{K'}$$

$$\frac{T_{e,k+1}^*(s)}{T_{e,k+1}(s)} = \left(\frac{K'k_p s + K'k_i - s^2 - K_1 s}{K's}\right) * \frac{s}{k_p s + k_i}$$

$$\frac{T_{e,k+1}^*(s)}{T_{e,k+1}(s)} = \frac{K'k_p s + K'k_i - s^2 - K_1 s}{K'k_p s + K'k_i}$$

$$\frac{T_{e,k+1}(s)}{T_{e,k+1}^*(s)} = \frac{K'k_p s + K'k_i}{-s^2 + (K'k_p - K_1)s + K'k_i} \quad (41)$$

In the same manner, we get:

$$\frac{E_{e,k+1}(s)}{E_{e,k+1}^*(s)} = \frac{1.2(kk_p s + k_i)}{-s^2 + 1.2kk_p s + 1.2kk_i} \quad (42)$$

The denominator of both (41) and (42) controls the dynamics of the PI controllers, so it is known as the characteristic equation, its roots must be negative and real to make the system stable, then the following must be achieved:

$$-s^2 + (K'k_p - K_1)s + K'k_i = 0 \quad (43)$$

By multiplying (41) by (-1), we obtain:

$$s^2 + (K_1 - K'k_p)s - K'k_i = 0 \quad (44)$$

For second order system, the characteristic equation is expressed by:

$$s^2 + 2D\omega_n s + \omega_n^2 = 0 \quad (45)$$

Lastly, to evaluate the parameters k_p and k_i of the PI torque regulator, we must perform a comparison between the terms of (44) and (45), which results in:

$$k_p = \frac{K_1 - 2D\omega_n}{K'} \quad and \quad k_i = -\frac{\omega_n^2}{K'} \quad (46)$$

By performing the same previous steps for the denominator of (42), we can find the parameters k_p and k_i of the PI air-gap energy regulator, as follows:

$$k_p = \frac{-2D\omega_n}{1.2K} \quad and \quad k_i = -\frac{\omega_n^2}{1.2K} \quad (47)$$

Where (ω_n) is the natural frequency of the system and (D) is the damping factor.

    Figure 5, presents a schematic diagram for the proposed PVC approach, in which the actual rotor current components can be predicted utilizing equations (3), (4), (20) and (21); also, the predicted stator current components can be found in the same manner. Then, the actual values of the torque and the air-gap energy can be evaluated using (10) and (27), respectively. As stated previously, the reference rotor current components are obtained using PI load power regulator and PI load voltage regulator, respectively. After that, the reference torque can be calculated using (22), meanwhile, the reference air-gap energy can be formulated as:

$$E_{e,k+1}^* = 1.5p \frac{L_m}{\sigma L_s L_r} \left(\Psi_{ds,k+1}^* \Psi_{dr,k+1}^* + \Psi_{qs,k+1}^* \Psi_{qr,k+1}^* \right) \qquad (48)$$

Now, the torque and gap energy errors are fed to the designed PI torque and air-gap energy regulators, respectively to obtain the active voltage components $u'_{dr,k+1}$ and $u'_{qr,k+1}$, and then added to the compensation components $\Delta u_{dr,k+1}^{sv}$ and $\Delta u_{qr,k+1}^{sv}$ to find the reference rotor voltage components $u_{dr,k+1}^*$ and $u_{qr,k+1}^*$, which are fed with the actual rotor voltage components to the cost function.
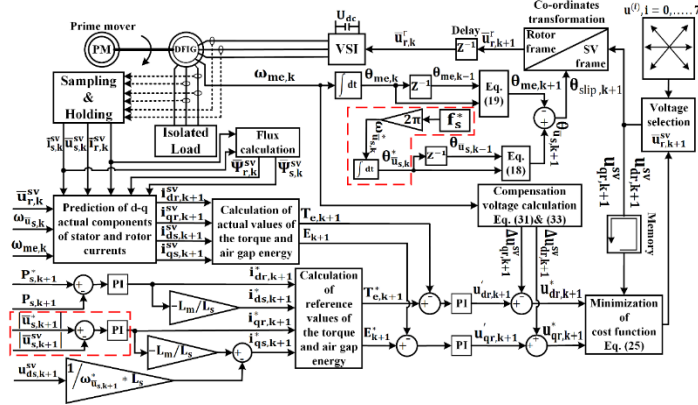
Figure 5: Scheme of proposed PVC strategy

4. Test results

The tests are performed for the three control approaches (SVOC, MPDTC and proposed PVC), using the MATLAB simulation (Simulink), through varying the reference active power $\left(P_{s,k}^*\right)$ and driving the DFIG by different operating wind speeds (super-synchronous and sub-synchronous), as shown in Figure 6. The reference power and operating speed are varied to evaluate the ability and robustness of each strategy during various operating regimes. The parameters of the DFIG and the model are introduced in Table A1, in Appendix A. The DFIG feeds an isolated load, which is a three-phase induction motor, and its parameters are presented in Table A2, in Appendix A.
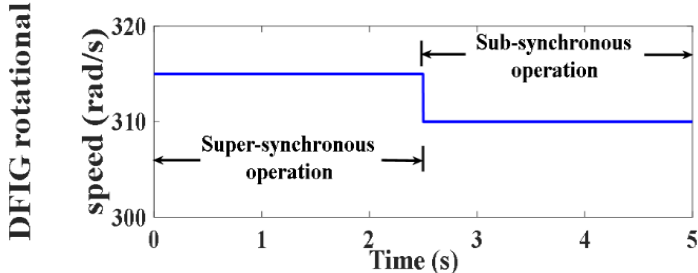
Figure 6: Prime mover operating speeds (rad/s)

4.1. Testing with SVOC technique

We performed the tests for the DFIG under SVOC principle to study its performance under the stated operating conditions. The obtained results are presented in Figures 7-16, which show

that the actual values follow their reference values smoothly. As known, the VOC is performed by independently controlling the torque current component $\left(i_{dr,k}^{sv}\right)$ and the field current component $\left(i_{qr,k}^{sv}\right)$; which is obvious through Figures 13 and 14, which confirm that the decoupling between the active and reactive current components has been achieved correctly. Furthermore, the active current component follows the active power and torque changes, while the reactive current component follows the reactive power and rotor flux changes. As noticed from the obtained results, the SVOC is ripple free which considered as the main merit of the SVOC. On the other hand, it suffers from system complexity, also, its dynamic response is slow due to using the PI current regulators.
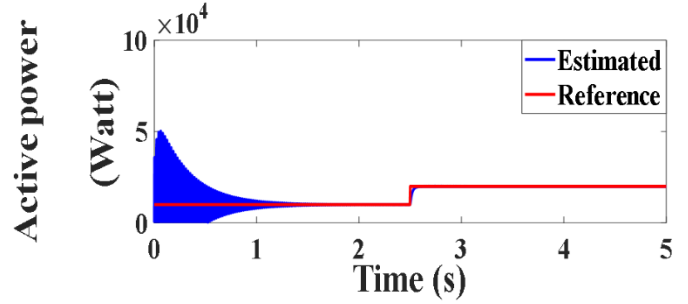
Figure 7: Active power under SVOC (Watt)
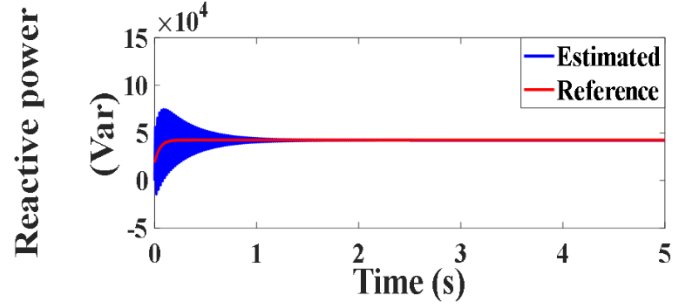
Figure 8: Reactive power under SVOC (Var)
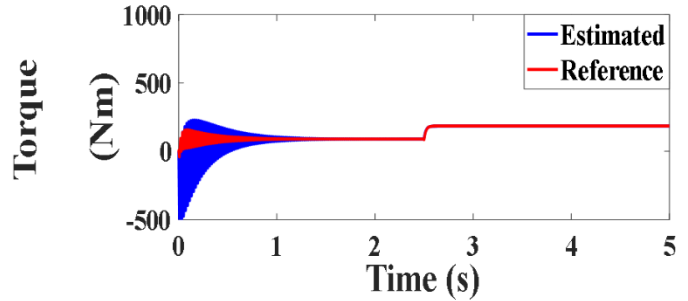
Figure 9: Torque developed under SVOC (Nm)
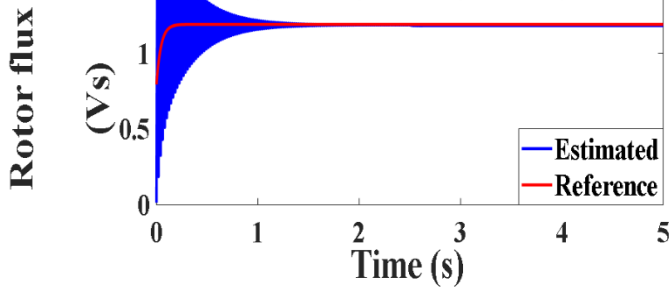
Figure 10: Rotor flux under SVOC (Vs)
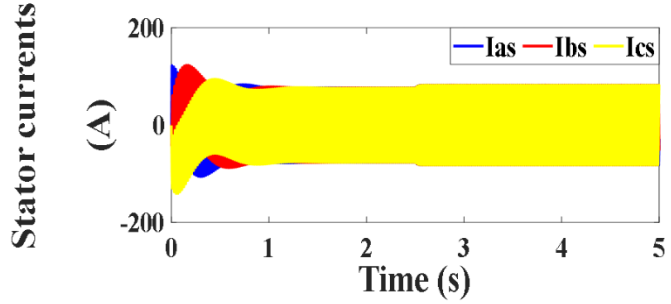
Figure 11: Stator currents under SVOC (A)
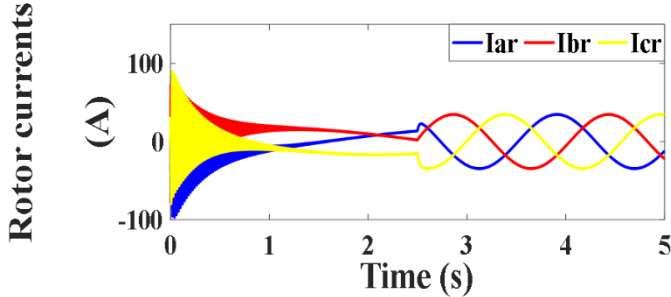
Figure 12: Rotor currents under SVOC (A)
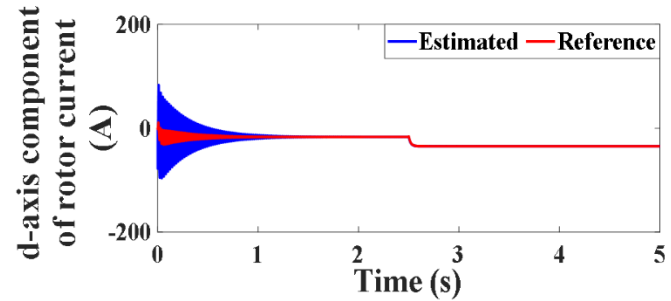
Figure 13: d-axis component of rotor current under SVOC (A)
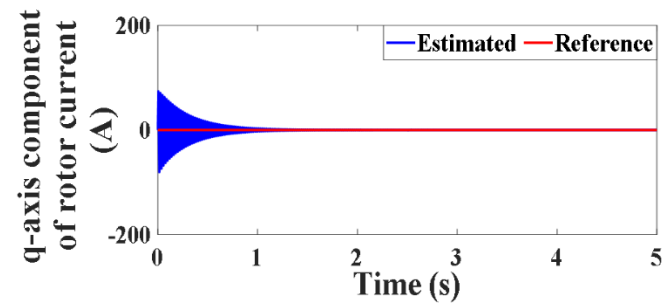
Figure 14: q-axis component of rotor current under SVOC (A)
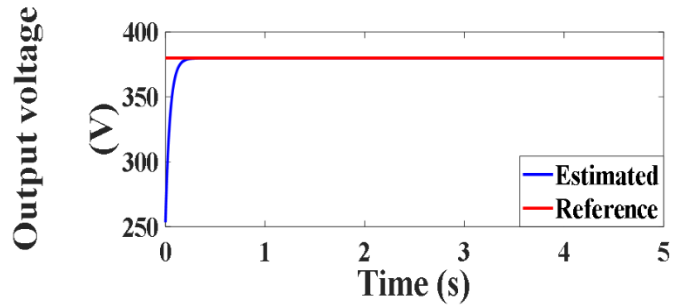
Figure 15: Load voltage under SVOC (V)
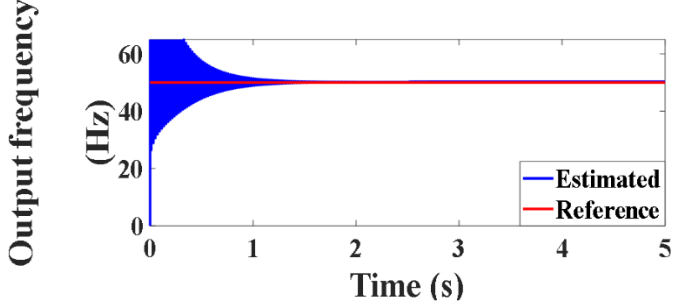
Figure 16: Load frequency under SVOC (Hz)

4.2. Testing with MPDTC technique

Tests for the DFIG's performance was performed under the MPDTC approach and the obtained results are shown in Figures 17-26, which illustrate that the actual values follow their reference values. Figures 23 and 24, show that the decoupling has been achieved between the current components. Furthermore, the torque component $\left(i_{dr,k}^{sv}\right)$ tracks the active power and torque changes, while the field component $\left(i_{qr,k}^{sv}\right)$ tracks the reactive power and rotor flux changes. The results reveal that the dynamic response of the MPDTC is faster than that of SVOC, but it has more ripples compared to SVOC.
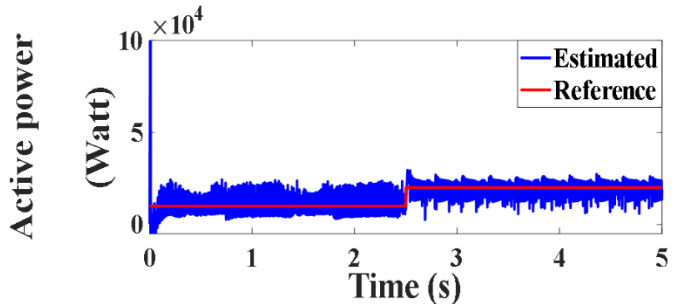
Figure 17: Active power under MPDTC (Watt)
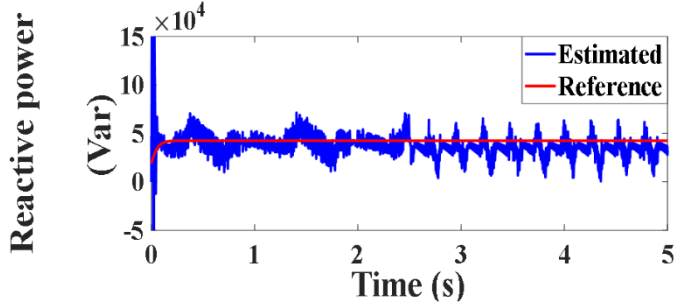
Figure 18: Reactive power under MPDTC (Var)
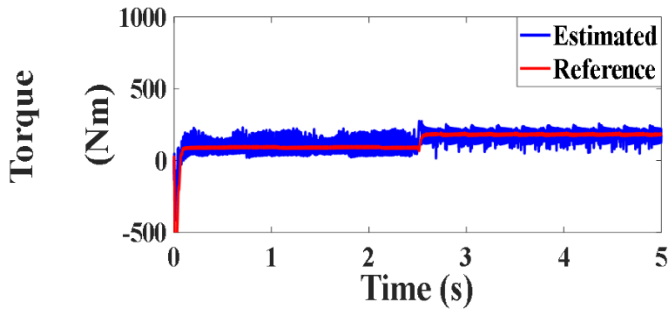
Figure 19: Torque developed under MPDTC (Nm)
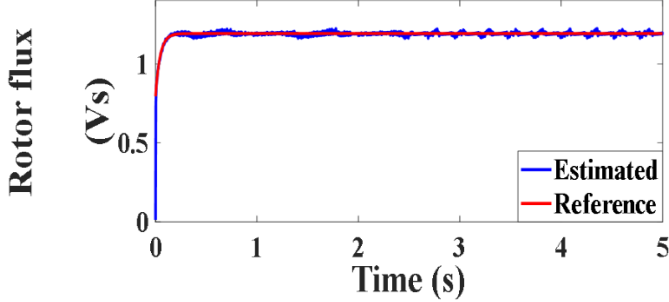
Figure 20: Rotor flux under MPDTC (Vs)
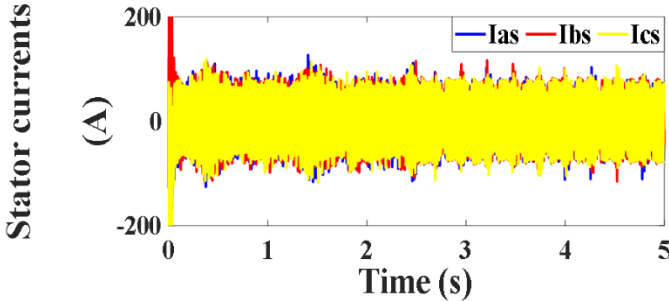
Figure 21: Stator currents under MPDTC (A)
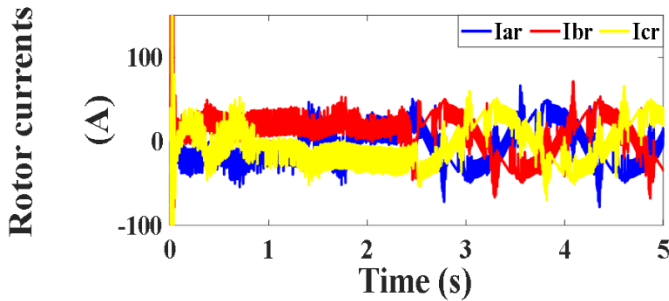
Figure 22: Rotor currents under MPDTC (A)
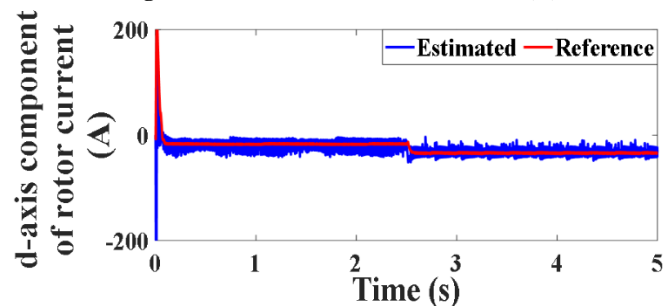
Figure 23: d-axis component of rotor current under MPDTC (A)
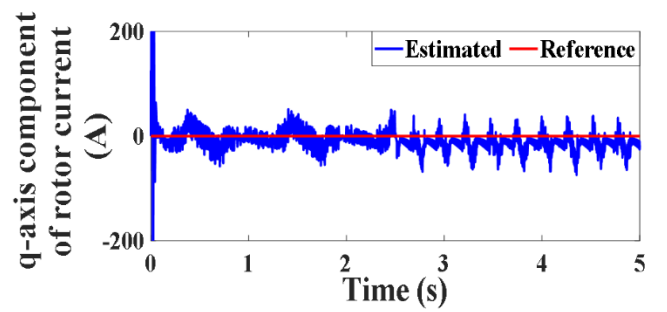
Figure 24: q-axis component of rotor current under MPDTC (A)
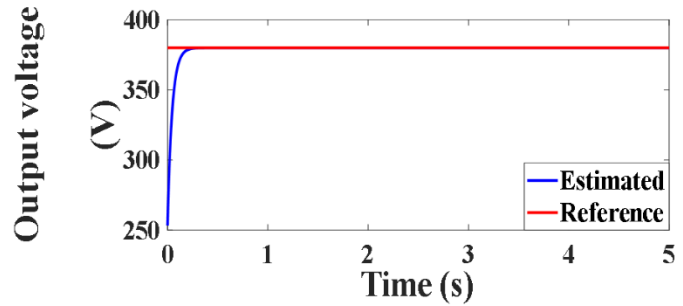
Figure 25: Load voltage under MPDTC (V)
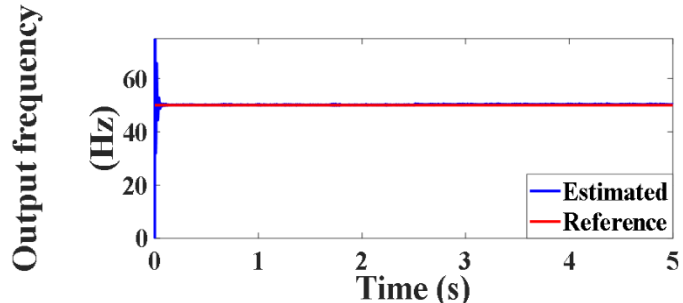
Figure 26: Load frequency under MPDTC (Hz)

4.3. Testing with proposed PVC technique

The DFIG was tested under the proposed PVC strategy to evaluate its performance. The results are presented in Figures 27-30, which clarify that the actual values of the active power, reactive power, developed torque and rotor flux keep track of their reference values. Furthermore, the stator and rotor currents follow the power change, as shown in Figures 31 and 32. The decoupling has been achieved correctly between the active and reactive current components as shown in Figures 13 and 14. Moreover, the direct current component follows the active power and torque changes, while the quadrature current component follows the reactive power and rotor flux changes. In addition, Figures 35 and 36, verify the ability of the control system to ensure a load voltage with constant amplitude and frequency irrespective of the power and speed changes. The results illustrate and prove the effectiveness of the formulated technique, as, it has the fastest dynamic response compared to MPDTC and SVOC techniques, moreover, its ripples' content is lower compared with that of MPDTC algorithm.

202

Figures 37-40, introduce the obtained results related to the load (IM), which are the motor torque, motor speed, motor stator flux and motor iso stator flux.
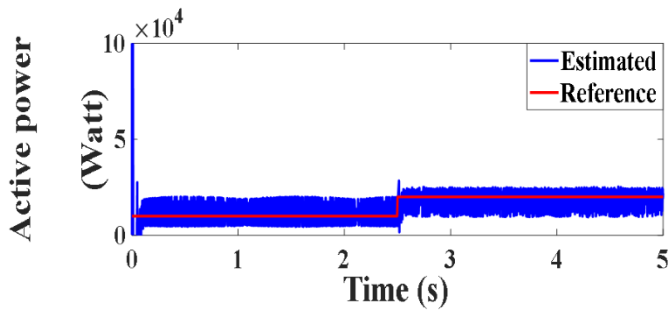
Figure 27: Active power under PVC (Watt)
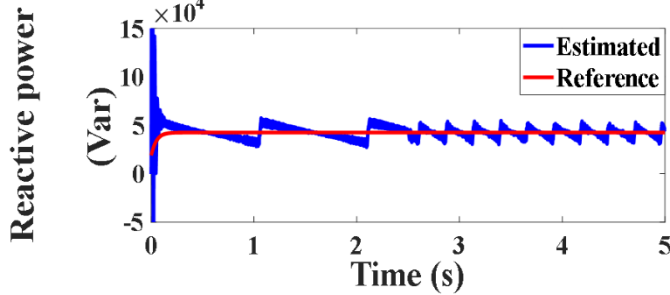
Figure 28: Reactive power under PVC (Var)
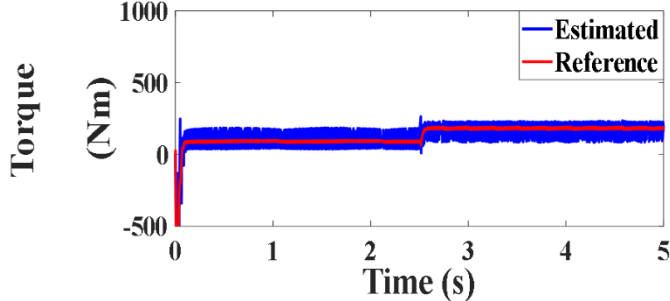
Figure 29: Torque developed under PVC (Nm)
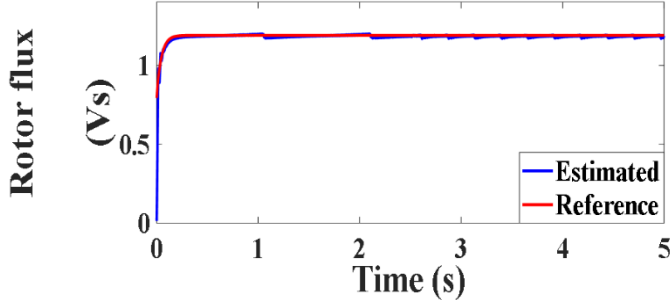
Figure 30: Rotor flux under PVC (Vs)
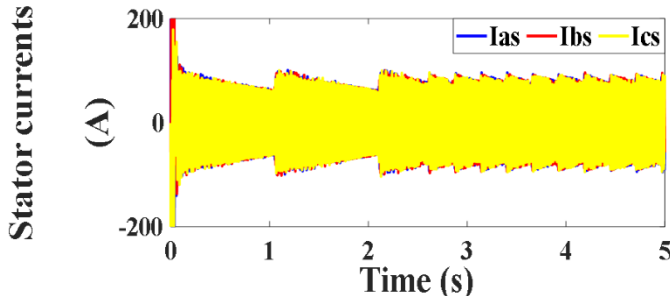
Figure 31: Stator currents under PVC (A)
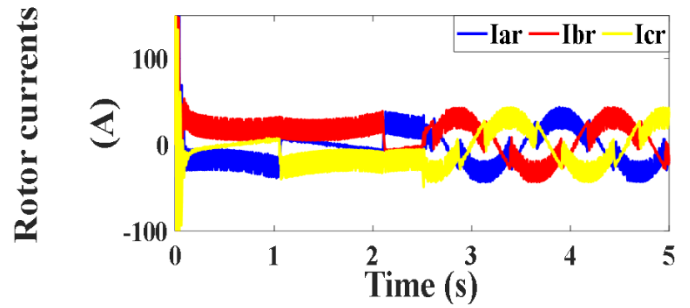
Figure 32: Rotor currents under PVC (A)
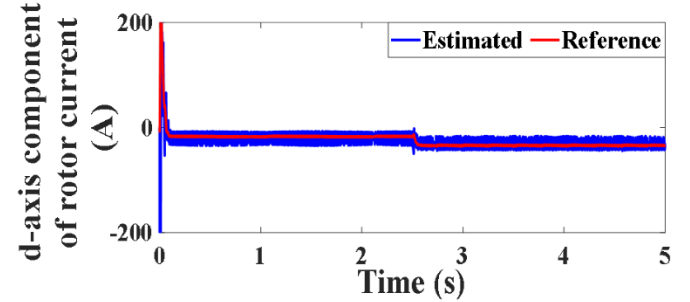
Figure 33: d-axis component of rotor current under PVC (A)
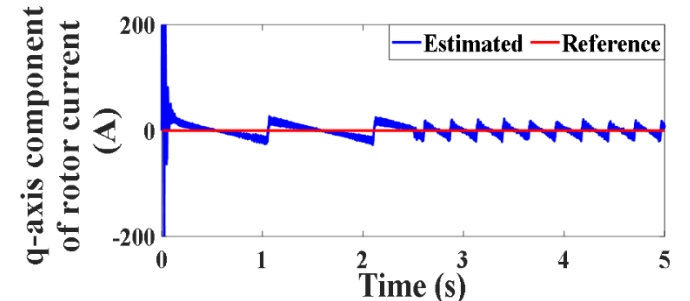
Figure 34: q-axis component of rotor current under PVC (A)
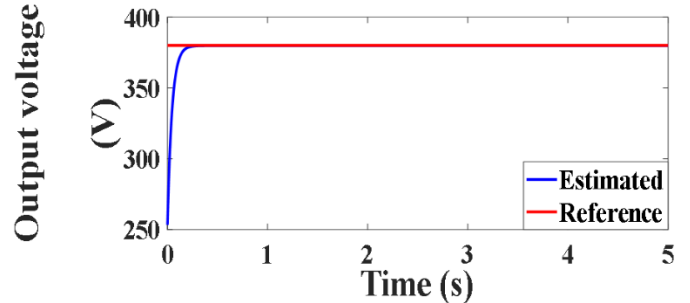
Figure 35: Load voltage under PVC (V)
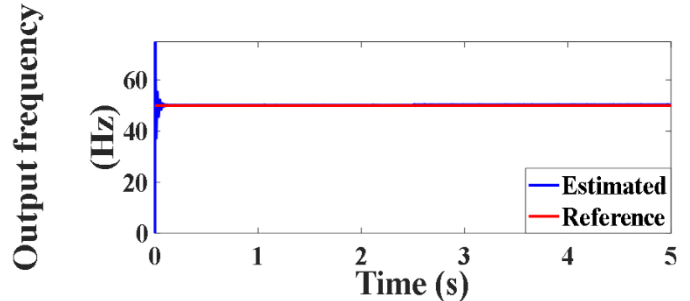
Figure 36: Load frequency under PVC (Hz)
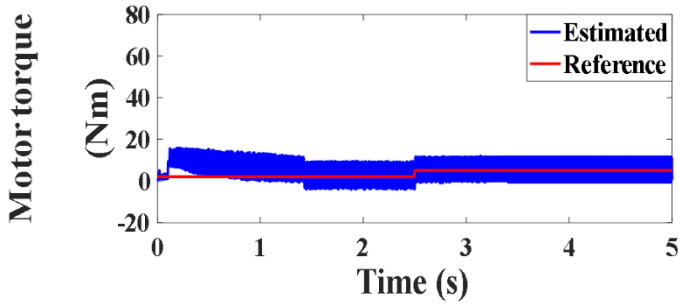
Figure 37: Motor torque (Nm)
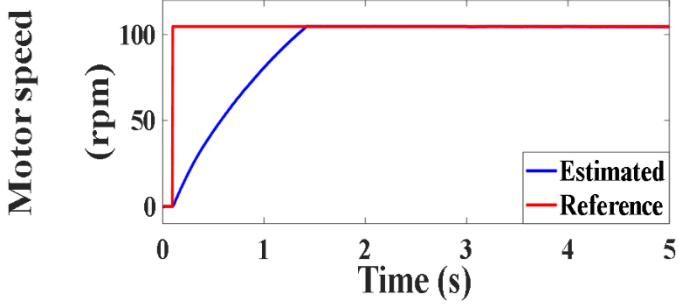
Figure 38: Motor speed (rpm)
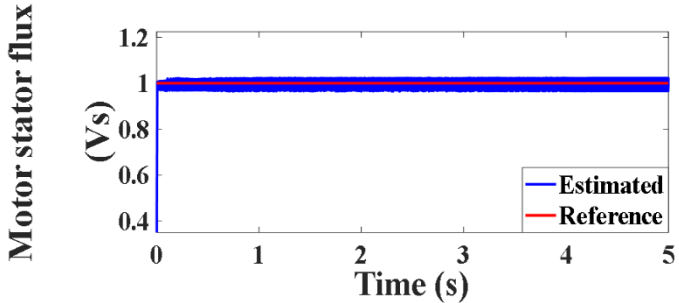
Figure 39: Motor stator flux (Vs)
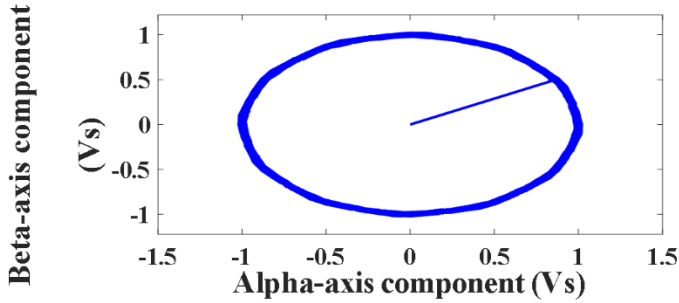
Figure 40: Motor iso stator flux (Vs)

4.4. Comparison study

Lastly, we perform a comprehensive comparison between the proposed PVC control scheme which designed in details in our paper and the classic control approaches (SVOC and MPDTC) to confirm the validation and effectiveness of our proposed scheme. The techniques' effectiveness was evaluated in terms of dynamic response time, ripples' content and total harmonic distortion (THD). The obtained results are shown in Figures 41-44, which visualize a comprehensive comparison among the three methodologies. Table 1, presents a comparison of the dynamic response time for each algorithm to determine which

technique takes shorter time to response to the power and speed changes, and therefore easily determine the fastest strategy in dynamic response. The results of Table 1, illustrate and confirm that the designed PVC scheme is the fastest dynamic response compared to other adopted controllers, as it takes the shortest response time. Table 2, introduces a detailed comparison for the three utilized controllers in terms of the ripples' content, and the results reveal that the content of ripples of PVC is lower than that of MPDTC algorithm.
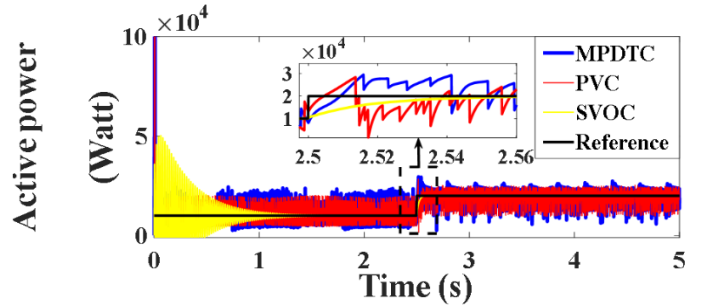
Figure 41: Active power (Watt)
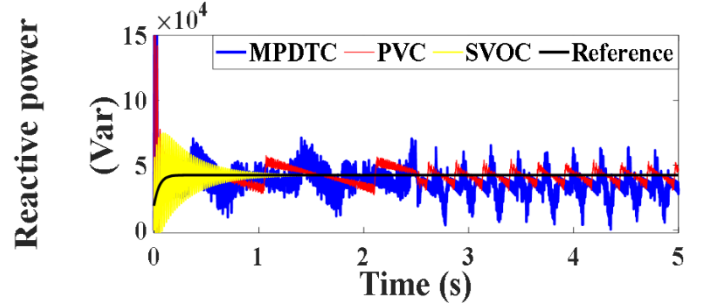
Figure 42: Reactive power (Var)
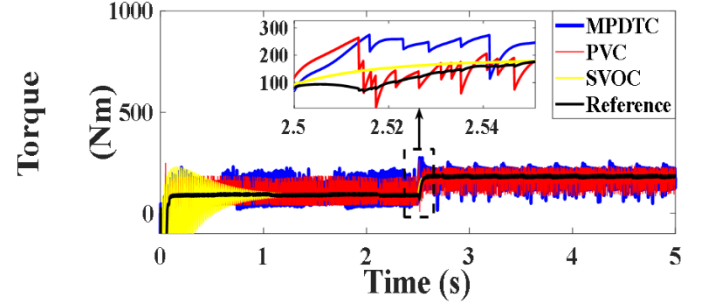
Figure 43: Developed torque (Nm)
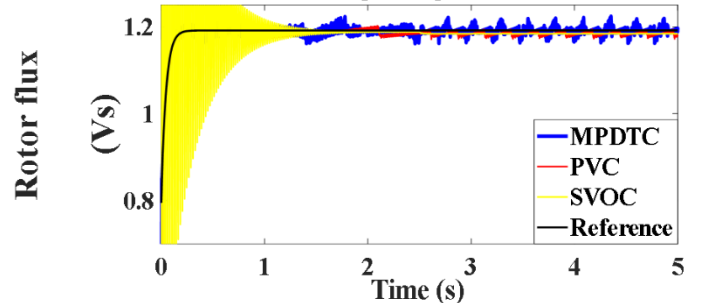
Figure 44: Rotor flux (Vs)

Table 1: Dynamic response time taken by the actual values to track their references

Technique	Time taken by the active power profile (s)	Time taken by the torque profile (s)
SVOC	0.053	0.05
MPDTC	0.009	0.041
PVC	0.004	0.015

Table 2: Ripples' content of the actual values above their references

Technique	Ripples of active power (Watt)	Ripples of reactive power (Var)	Ripples of developed torque (Nm)	Ripples of rotor flux (Vs)
SVOC	860	280	5	0.008
MPDTC	9470	28770	90	0.032
PVC	3950	7160	40	0.01

The FFT analysis for the stator current components under the MPDTC and proposed PVC are presented in Figures 45-50, which clarifies and proves the superiority of the designed PVC over the MPDTC, as it has lower THD, which proved also by the numerical values in Table 3. Therefore, it can be concluded that the proposed PVC strategy is the most convenient approach to be utilized with the DFIG; as it eliminates the system complexity; it is considered as the fastest dynamic response compared to MPDTC and SVOC; it has lower ripples' content compared with that of MPDTC; and it has lower THD than that of MPDTC technique.
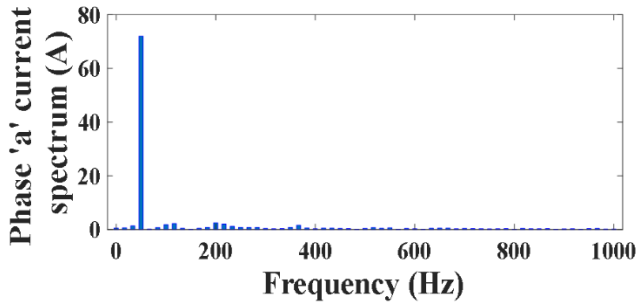
Figure 45: Spectrum of Phase "a" of stator current under MPDTC
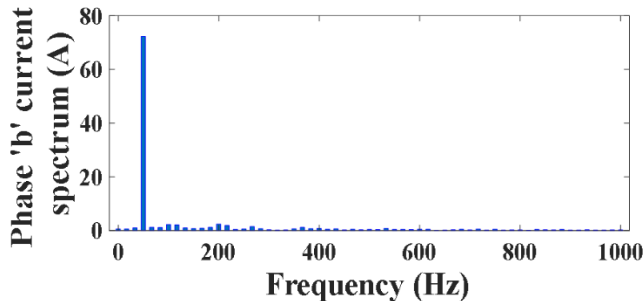
Figure 46: Spectrum of Phase "b" of stator current under MPDTC
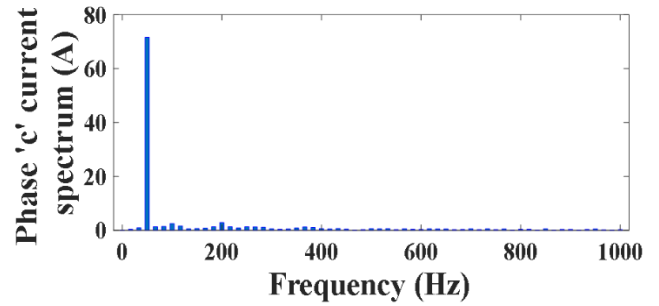
Figure 47: Spectrum of Phase "c" of stator current under MPDTC
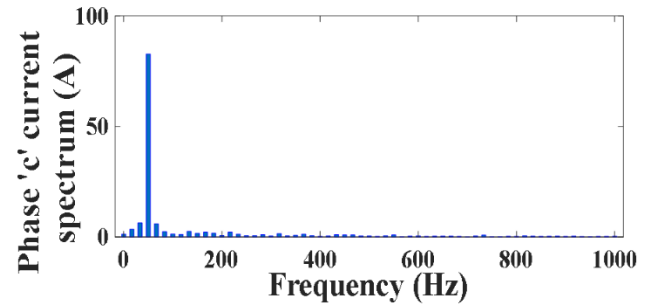
Figure 48: Spectrum of Phase "a" of stator current under PVC
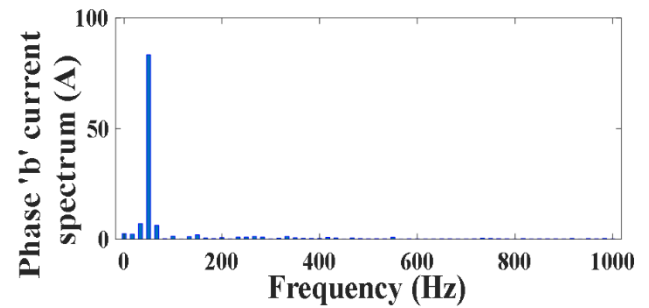
Figure 49: Spectrum of Phase "b" of stator current under PVC
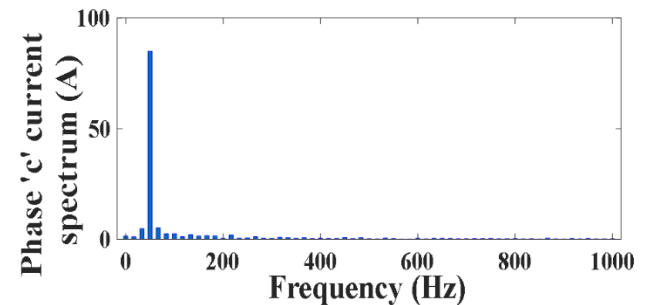
Figure 50: Spectrum of Phase "c" of stator current under PVC

Table 3: FFT analysis for the stator current components

	MPDTC		PVC	
	Fundamental	THD	Fundamental	THD
Phase A	71.9962 A	4.79 %	82.8134 A	3.22 %
Phase B	72.2762 A	5.09 %	83.3904 A	3.65 %
Phase C	71.5451 A	5.87 %	85.0379 A	3.72 %

5. Conclusions

The present article has managed to introduce a detailed analysis for the dynamic performance of the DFIG utilizing

various control approaches under varying the operating speeds and perform a comprehensive comparison for the performance of the DFIG under the utilized controllers. The control schemes which adopted in this paper, are stator voltage-oriented control (SVOC), model predictive direct torque control (MPDTC) as conventional controllers and a newly designed predictive voltage control (PVC) scheme as an improved type. The formulated PVC approach has presented better dynamic performance compared to other controllers; as, its cost function is very simple compared to MPDTC because it doesn't require a weighting scale, also, the variables utilized in the cost function don't depend on the machine parameters. Furthermore, the comparison results reveal and prove that, the proposed PVC scheme has lower ripples compared to MPDTC, and its dynamic response is faster than that of MPDTC and SVCO techniques. Moreover, the proposed PVC scheme introduces a lower THD than that of MPDTC, which means that, the formulated PVC scheme is the most appropriate control method to be adopted with the DFIG.

Conflict of Interest

The authors declare no conflict of interest.

Appendix A

Table A1: Data specification

Parameter	Value	Parameter	Value
R_s	0.07 Ω	Rated power	55 Kw
R_r	0.087 Ω	Stator rated voltage	380 V
Ls	0.01625 H	Operating frequency	50 Hz
Lr	0.0163 H	Sampling time	100 μs
L_m	0.016 H	DC link voltage (U_{dc})	570 v
Pole pairs (p)	3	K_p and K_i (Active power regulator)	0.0001 and -0.1
Inertia	0.1 kg.m^2	K_p and K_i (Stator voltage regulator)	0.01 and -20

Table A2: Parameters of IM

Parameter	Value	Parameter	Value
R_s	1.5 Ω	L_m	0.17447 H
R_r	0.85 Ω	Rated power	3 Kw
Ls	0.1785 H	Pole pairs (p)	1
Lr	0.18451 H	Inertia	0.06 kg.m^2

References

[1] J. R. Andrade and R. J. Bessa, "Improving Renewable Energy Forecasting With a Grid of Numerical Weather Predictions," *IEEE Transactions on Sustainable Energy,* vol. 8, no. 4, pp. 1571-1580, 2017.

[2] R. Pena, J. C. Clare, and G. M. Asher, "Doubly fed induction generator using back-to-back PWM converters and its application to variable-speed wind-energy generation," *IEE Proceedings - Electric Power Applications*, vol. 143, no. 3, pp. 231-241.

[3] M. A. Mossa, O. Gam, N. Bianchi, et al, "Enhanced Control and Power Management for a Renewable Energy-Based Water Pumping System," *IEEE Access,* vol. 10, pp. 36028-36056, 2022.

[4] A. A. Hassan, A. M. El-Sawy, and O. M. Kamel, "Direct Torque Control of a Doubly fed Induction Generator Driven By a Variable Speed Wind Turbine," (in en), *JES. Journal of Engineering Sciences,* vol. 41, no. No 1, pp. 199-216, 2013.

[5] M. G. Stohy, H. S. Abbas, A.-H. M. El-Sayed, et al, "PARAMETER ESTIMATION AND PI CONTROL FOR A WATER COUPLED TANK SYSTEM," (in en), *Journal of Advanced Engineering Trends,* vol. 38, no. 2, pp. 147-159, 2020.

[6] C. M. R. Charles, V. Vinod, and A. Jacob, "Field Oriented Control of DFIG Based Wind Energy System Using Battery Energy Storage System," *Procedia Technology,* vol. 24, pp. 1203-1210, 2016/01/01/ 2016.

[7] M. A. Mossa, H. Echeikh, and A. Iqbal, "Enhanced control technique for a sensor-less wind driven doubly fed induction generator for energy conversion purpose," *Energy Reports,* vol. 7, pp. 5815-5833, 2021/11/01/ 2021.

[8] S. Mahfoud, A. Derouich, N. El Ouanjli, et al, "A New Strategy-Based PID Controller Optimized by Genetic Algorithm for DTC of the Doubly Fed Induction Motor," *Systems,* vol. 9, no. 2, 2021.

[9] R. A. J. Amalorpavaraj, P. Kaliannan, S. Padmanaban, et al, "Improved Fault Ride Through Capability in DFIG Based Wind Turbines Using Dynamic Voltage Restorer With Combined Feed-Forward and Feed-Back Control," *IEEE Access,* vol. 5, pp. 20494-20503, 2017.

[10] M. A. Mossa, M. K. Abdelhamid, A. A. Hassan, et al, "Improving the Dynamic Performance of a Variable Speed DFIG for Energy Conversion Purposes Using an Effective Control System," *Processes,* vol. 10, no. 3, 2022.

[11] M. A. Mossa, H. Echeikh, A. A. Z. Diab, et al, "Effective Direct Power Control for a Sensor-Less Doubly Fed Induction Generator with a Losses Minimization Criterion," *Electronics,* vol. 9, no. 8, 2020.

[12] L. Dambrosio and B. Fortunato, "One-step-ahead adaptive control of a wind-driven, synchronous generator system," *Energy,* vol. 24, no. 1, pp. 9-20, 1999/01/01/ 1999.

[13] R. M. Prasad and M. A. Mulla, "Mathematical Modeling and Position-Sensorless Algorithm for Stator-Side Field-Oriented Control of Rotor-Tied DFIG in Rotor Flux Reference Frame," *IEEE Transactions on Energy Conversion,* vol. 35, no. 2, pp. 631-639, 2020.

[14] M. A. Mossa, A. S. Al-Sumaiti, T. D. Do, et al, "Cost-Effective Predictive Flux Control for a Sensorless Doubly Fed Induction Generator," *IEEE Access,* vol. 7, pp. 172606-172627, 2019.

[15] M. A. Mossa, O. Gam, and N. Bianchi, "Dynamic Performance Enhancement of a Renewable Energy System for Grid Connection and Stand-alone Operation with Battery Storage," *Energies,* vol. 15, no. 3, 2022.

[16] M. R. M. Hassan, M. A. Mossa, and G. M. Dousoky, "Evaluation of Electric Dynamic Performance of an Electric Vehicle System Using Different Control Techniques," *Electronics,* vol. 10, no. 21, 2021.

[17] A. Gundavarapu, H. Misra, and A. K. Jain, "Direct Torque Control Scheme for DC Voltage Regulation of the Standalone DFIG-DC System," *IEEE Transactions on Industrial Electronics,* vol. 64, no. 5, pp. 3502-3512, 2017.

[18] M. R. A. Kashkooli, S. M. Madani, and T. A. Lipo, "Improved Direct Torque Control for a DFIG under Symmetrical Voltage Dip With Transient Flux Damping," *IEEE Transactions on Industrial Electronics,* vol. 67, no. 1, pp. 28-37, 2020.

[19] M. A. Mossa, T. D. Do, A. S. Al-Sumaiti, et al, "Effective Model Predictive Voltage Control for a Sensorless Doubly Fed Induction Generator," *IEEE Canadian Journal of Electrical and Computer Engineering,* vol. 44, no. 1, pp. 50-64, 2021.

[20] M. A. Mossa, T. D. Do, H. Echeikh, et al, "A Predictive Voltage Control Scheme For A Variable Speed Doubly Fed Induction Generator," in *2021 IEEE 12th Energy Conversion Congress & Exposition-Asia (ECCE-Asia)*, 2021, pp. 1491-1497: IEEE.

[21] A. A. Hassan, Y. S. Mohamed, A. M. El-Sawy, et al, "Control of a Wind Driven DFIG Connected to the Grid Based on Field Orientation," *Wind Engineering,* vol. 35, no. 2, pp. 127-143, 2011/04/01 2011.

[22] P. Pura and G. Iwański, "Rotor Current Feedback Based Direct Power Control of a Doubly Fed Induction Generator Operating with Unbalanced Grid," *Energies,* vol. 14, no. 11, 2021.

[23] Q. Huang, X. Zou, D. Zhu, et al, "Scaled Current Tracking Control for Doubly Fed Induction Generator to Ride-Through Serious Grid Faults," *IEEE Transactions on Power Electronics,* vol. 31, no. 3, pp. 2150-2165, 2016.